TECHNICAL DESCRIPTION OF THE PERMAFROST WATER BALANCE MODEL VERSION 4.0

Michael A. Rawlins

Climate System Research Center
University of Massachusetts
Amherst, MA 01003

Contents

The Permafrost Water Balance Model (PWBM, Figure 1) is a hydrologic model descended from the Water Balance Model (WBM) (Vörösmarty et al., 1998). It is designed for application in northern high latitude regions. The PWBM uses meteorological forcings at an implicit daily time step and produces outputs of snow mass, runoff, evapotranspiration and other model simulated water storages and fluxes. It was recently extended to simulate the loading of dissolved organic carbon to rivers systems over the chosen model domain (Rawlins et al., 2021). Details of the algorithms for major components of PWBM version 4 are described below.

1. Snow Dynamics

1.1. **Snow sublimation.** Daily precipitation for each grid is partitioned into either rain or snow based on a daily air temperature threshold (t_{thresh}). The simulated snowpack contains both a solid (frozen) and liquid portion, providing a total model value for snow water equivalent (SWE). Sublimation from the frozen snow can be determined through a simple function (Hamon, 1963), which allows for a small amount of sublimation at air temperatures below freezing.

$$B_t = 715.5\,\Lambda\, e*(T_t)\,/\,(T_t + 273.2) \tag{1}$$

where B_t is sublimation (or potential evapotranspiration (PET) when snow is absent) (mm day^{-1}) on day t, Λ is daylength (fraction of day), and $e*(T_t)$ is daily saturated vapor pressure (kPa) at temperature T_t (°C). As of PWBM version 4 (Rawlins et al., 2021), daily values of snow sublimation are estimated through a modification to B_t based on land cover class and independent estimates of leaf area index (LAI). Daily snow sublimation ($S_{subl,t}$, mm day^{-1}) is computed as

$$S_{sub,t} = B_t \cdot G_t \tag{2}$$

where G_t is a dimensionless scalar that takes the form

$$G_t = \begin{cases} SWE_t\ k_{subl,T}, & for\ \text{tundra} \\ SWE_t\ k_{subl,F}, & for\ \text{forest, LAI} < 1.0 \\ SWE_t\ (k_{subl,F} + LAI), & for\ \text{forest, LAI} \geq 1.0 \end{cases} \tag{3}$$

where SWE_t is the model value for snow water equivalent (mm), LAI is monthly average leaf area index (m^2 m^{-2}), $k_{subl,T}$ is the calibration coefficient for tundra, and $k_{subl,F}$ is the calibration coefficient for forest environments. The variation imposed by changing LAI in forest areas when LAI $\geq$ 1.0 accounts for the influence of canopy interception on sublimation, with higher LAI resulting in less snow mass at the surface. Monthly long-term mean LAI are used in the algorithm, for example, from the Advanced Very High Resolution Radiometer (AVHRR) Global Inventory Modeling and Mapping Studies (GIMMS) LAI3g version 2 (Mao and Yan, 2019).

1.2. **Snowpack evolution.** The snow model in PWBM incorporates approaches described in Liston et al. (2007) and Schaefer et al. (2009), and incorporates the Sturm et al. (1995) snow classification. To resolve temperature dynamics, the snow model simulates up to five layers depending on total depth. The bottom layer is thickest, with decreasing layer thickness moving upward. Within this framework a two layer density

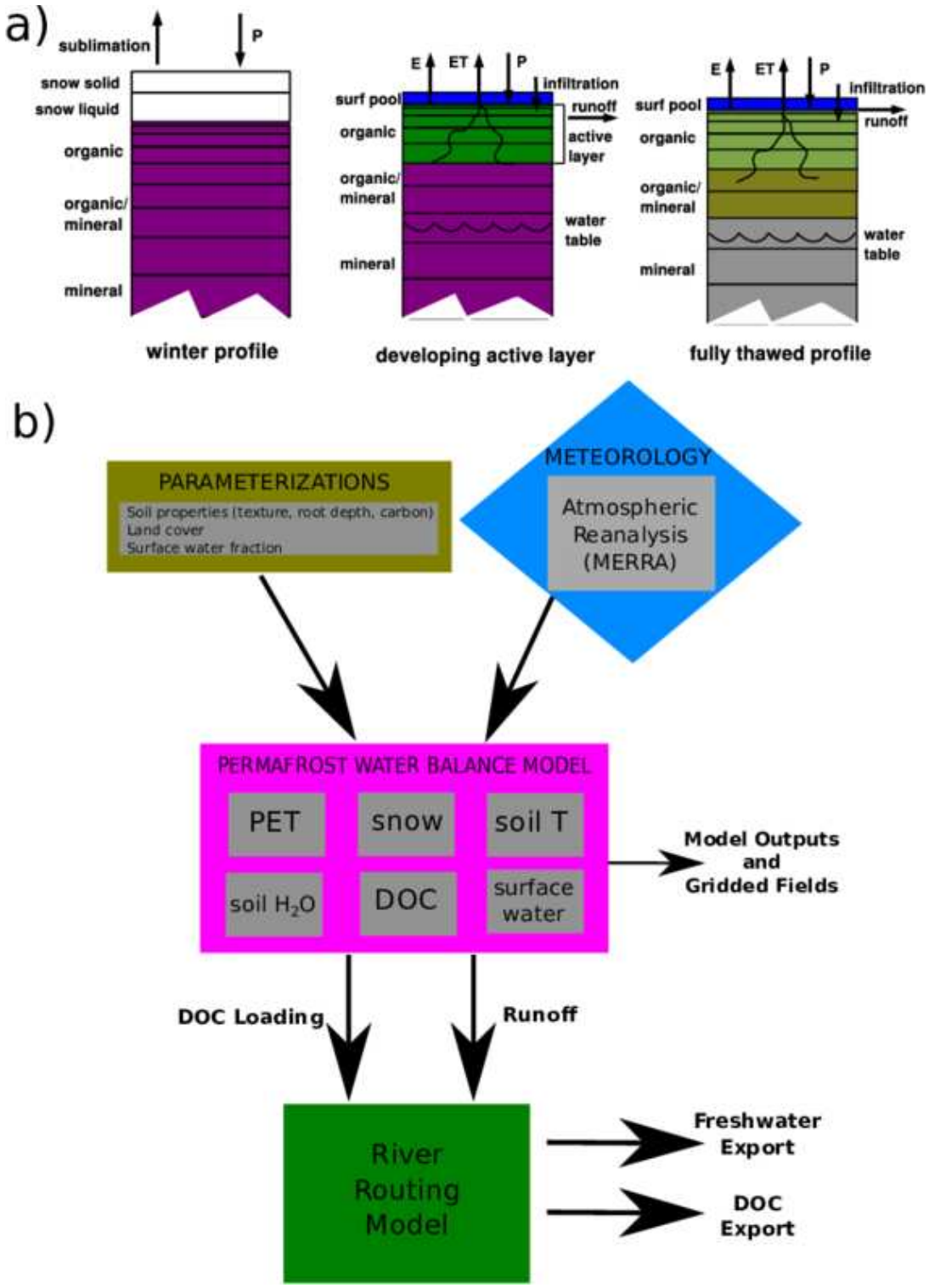

FIGURE 1. a) Schematic diagram of the vertical profiles for the Permafrost Water Balance Model (PWBM) showing characteristic water storage and flux elements for winter, late spring when active layer is developing, and a thawed profile consistent with summer in an area absent of permafrost. b) Flowchart showing model parameterizations, forcings, outputs, and submodules. River routing of DOC mass loading is not employed in the present study.

model (Schaefer et al., 2009) is imposed. The relative thickness of the bottom depth hoar layer (f_{bot}) is a function of total snowpack depth

$$f_{bot} = f_{botmax}/(1 + exp(D_{slope}(D_{half} - D))) \tag{4}$$

where f_{botmax} is the maximum potential thickness for the depth hoar layer and D_{slope} and D_{half} are f_{bot} slope and half point

$$D_{half} = (D_{max} + D_{min})/2$$

$$D_{slope} = 10/(D_{max} + D_{min}) \tag{5}$$

Here D_{min} is the minimum depth where a bottom layer forms and D_{max} is the depth where f_{bot} is its maximum value. Within the global snow classification of Sturm et al. (1995) only tundra and taiga types occur across the pan-Arctic drainage basin. For tundra grids D_{min}, D_{max}, f_{botmax} are 0.0, 0.1, 0.3, respectively (Schaefer et al., 2009). For taiga snow they are 0.0, 0.7, 0.7. Due to the special properties of the depth hoar layer in tundra and taiga environments we assume thermal conductivity (λ_{dh}) in this layer as 0.18 and 0.072 W m^{-2} K^{-1}, respectively. Temporal evolution of density in the upper 'soft snow' layer are calculated based on the approach described in Liston et al. (2007), wherein snow density is influenced primarily through snow precipitation and compaction as a result of wind. New snow density is defined

$$\rho_{ns} = \rho_0 + 1.7(T_a - 258.16)^{1.5} \tag{6}$$

where T_a is air temperature and ρ_0 is fresh snow. Here we use a value of 100 kg m^{-3} as opposed to the 50 kg m^{-3} applied in Liston et al. (2007). A density offset is added for wind speeds > 5 m s^{-1}. During periods of no precipitation snow density evolution is given by

$$\frac{d\rho_s}{dt} = CA_1U\rho_s exp[-B(T_f - T_s)]exp(-A_2\rho_s) \tag{7}$$

where T_f is freezing temperature, T_s is soft snow temperature, B is a constant equal to 0.08 K^{-1}, A_1 and A_2 are constants set to 0.0013 m^{-1} and 0.021 m^3 kg^{-1}, respectively, and $C = 0.10$ is a constant that controls the snow density change rate. Thermal conductivity of the upper snow layer for both tundra and taiga classes is

$$\lambda_{eff} = 0.138 - 1.01\rho_s + 3.233\rho^2 \tag{8}$$

where λ_{eff} is in W m^{-1} K^{-1} and ρ_s is snow density in kg m^{-3} (Sturm et al., 1997). We assumed a thermal conductivity in the lower depth hoar layer of 0.18 W m^{-1} K^{-1} for tundra snow and 0.072 W m^{-1} K^{-1} for taiga snow. Finally, the snow thickness $z_s = z_s(t)$ is computed simply using the model estimate for snow water equivalent (SWE) and snow density $z_s(t) = W/\rho_s$).

1.3. **Determination of snow layers.** We discretize a space above the ground surface into 5 fixed layers x_{-5}=−0.70m, x_{-4}=−0.45m, x_{-3}=−0.30m, x_{-2}=−0.15m, and x_{-1}=−0.07m. For example when the snow pack thickness x_s is 0.3m, then the snow consists of three layers x_{-3}, x_{-2}, x_{-1}. However, when snow starts to accumulate then the snowpack thickness x_s increases and it exceeds x_{-3}. To take into account this fresh snow, the value of x_{-3} is dynamically adjusted to become the current snow thickness. Note that the number of snow layers is still equal to 3. However, when the snowpack

thickness becomes larger than $(x_{-3} + x_{-4})/2$, then the snowpack starts to have 4 layers: x_{-1}=−0.07, x_{-2}=−0.15, x_{-3}=−0.30, and $x_{-4} = x_s$.

1.4. **Snowmelt.** Daily snowmelt, a function of rainfall and/or air temperature, is computed as

$$M_t = f_v \cdot \left(2.63 + 2.55\,T_t + 0.0912\,T_t\,P_t\right) \tag{9}$$

where M_t is snowmelt (mm day^{-1}), f_v is a vegetation factor that accounts for the differential absorption of radiation for different landcover types (dimensionless, range 0.4 to 1.0) (Federer and Lash, 1978), T_t represents daily air temperature (°C) and P_t is precipitation (mm day^{-1}), all on day t (Willmott et al., 1985). Snowmelt and/or rainfall contributes to the liquid portion of the snowpack. Damming of snowmelt runoff is a complex process which delays the timing of streamflow during spring (Hinzman and Kane, 1991). The snowpack is assumed to retain liquid water (SWE_l) until the liquid content exceeds a threshold ($k_{swehold}$) of the snowpack frozen water amount (SWE_s), whereupon a fraction (k_{sweout}) of the liquid water is released to the soil surface. Both $k_{swehold}$ and k_{sweout} represent all processes that delay the release and movement of snowpack water to river networks. This process is determined through

$$AW_t = \begin{cases} SW_t\,k_{sweout}\,, & SWE_l \geq k_{swehold}\,SWE_s \\ 0, & \text{otherwise} \end{cases} \tag{10}$$

where AW_t is water made available to the soil surface (mm day^{-1}).

2. Soil Temperature and Moisture

2.1. **Stefan solution for phase change.** The earliest version of the PWBM used the Stefan solution of heat transfer with phase change in a uniform semi-infinite medium (Lunardini, 1981) to approximate soil temperatures and, in turn, soil liquid water and ice contents

$$z(t) = \sqrt{\frac{2\,k\,(n\,DDT(t))}{w\,\rho_b\,L}} \tag{11}$$

where z_t is the depth of the phase change boundary (m), k is the soil thermal conductivity above the phase change boundary (J m^{-1} C^{-1} d^{-1}), n is the n-factor, relating integrated air temperature to integrated soil-surface temperature (Lunardini, 1978) (dimensionless), $DDT(t)$ is the accumulated degree days of thaw (or freeze) (°C-day), w is the soil water content at the phase change boundary (kg kg^{-1} dry soil), ρ_b is the soil bulk density (kg m^{-3}), and L is the latent heat of fusion of water (J kg^{-1}).

TABLE 1. Soil parameters used in the PWBM simulations. Values shown are for thermal conductivity (λ), heat capacity (C), saturated hydraulic conductivity (k_{sat}), porosity (θ_{sat}), soil bulk density (ρ_b), field capacity (FC), wilting point (WP), soil hydraulic matrix potential (Ψ_{sat}), and the soil texture parameter (β). Each grid cell in the model is characterized by one of the five mineral soil types. Model parameters are defined through a weighted combination of organic and mineral soil properties. See Rawlins et al. (2003), Rawlins et al. (2013), and Rawlins et al. (2021) for more detail on the PWBM soil algorithms and routines. Quantities with units of % are shown with values as decimal fractions from 0–1 (eg. 25% = 0.25).

Parameter	λ (W m^{-1} K^{-1})	C (J m^{-3} K^{-1} $\times$ 10^6)	k_{sat} (m s^{-1} $\times$ 10^{-3})	Θ_{sat} (%)	ρ_b (g/cm^3)	FC (cm/cm^3)	WP (cm/cm^3)	Ψ_{sat} (mm)	β
sand	$\lambda_m = 3.6$	$C_m = 3.0$	0.023	0.30	1.60	0.05	0.04	-47	3.4
loam	$\lambda_m = 3.0$	$C_m = 3.0$	0.042	0.35	1.44	0.24	0.09	-207	6.1
clay	$\lambda_m = 2.3$	$C_m = 3.0$	0.020	0.45	1.21	0.35	0.09	-390	12.1
sandy loam	$\lambda_m = 3.3$	$C_m = 3.0$	0.071	0.40	1.35	0.32	0.17	-132	4.5
clay loam	$\lambda_m = 2.6$	$C_m = 3.0$	0.028	0.39	1.60	0.05	0.04	-289	8.2
organic soil	$\lambda_o = 1.5$	$C_o = 1.9$	0.02	0.90	1.3	0.65	0.10	-120	2.7

2.2. **1-D heat equation with phase change.** As of version 3 (Rawlins et al., 2013), soil temperatures are simulated by a 1-D heat equation with phase change (Carslaw, 1974). The newer algorithms were implemented to better account for the thermal and hydrologic properties of soils, and involve parameterization of soil carbon density in each soil layer. This involves a similar but not identical approach to the one described in Lawrence and Slater (2008). The PWBM soil model discretizes a 60 meter soil column into 23 layers (i), with layer thickness increasing with depth. The center of the layers are at depths (cm): 1, 3, 8, 13, 23, 33, 45, 55, 70, 105, 140, 175, 225, 275, 325, 475, 725, 1400, 2200, 3100, 4000, 5000, 6000.

The model simulates snow/ground temperature dynamics in a physically-based manner using the 1-D heat equation with phase change

$$C\frac{\partial T}{\partial t} + L\zeta\frac{\partial \theta}{\partial t} = \frac{\partial}{\partial z}\left(\lambda\frac{\partial T}{\partial z}\right), \qquad z \in [z_s, z_b] \tag{12}$$

and diffusive and gravitational movement of water in thawed ground by solving Richard's equation

$$\frac{\partial \zeta}{\partial t} = \frac{\partial}{\partial z}\left(k\left[\frac{\partial \psi}{\partial z} + 1\right]\right), \qquad z \in [0, z_b]. \tag{13}$$

Here $T = T(z,t)$ is the temperature, $\zeta = \zeta(z,t)$ is the volumetric water content, $\psi = \psi(z,t)$ is the soil matrix potential. The quantities C=$C(T,z)$ $[Jm^{-3}K^{-1}]$ and λ=$\lambda(T,z)$ $[Wm^{-1}K^{-1}]$ represents the volumetric heat capacity and thermal conductivity of soil, respectively; L $[Jm^{-3}]$ is the volumetric latent heat of fusion of water, and $\theta = \theta(T,z)$ is the so-called 'unfrozen liquid pore water' fraction, and k=$k(T,z)$ is the hydraulic conductivity. The equations are solved implicitly with a daily time step. At the upper boundary condition air temperature and precipitation are prescribed as described below. We emphasize that equation (13) is applicable only for the thawed ground material. In order to extend to simulations of water motion in frozen ground, some model algorithms require that $\psi = \psi(T,\theta,x)$ if $T < T_p$, where T_p is the so-called freezing-point temperature depression. In this work we assume that the water migration in the frozen ground is negligibly small. The latter can be modeled by assuming that the coefficient of hydraulic conductivity $k(T,z) = 0$, if $T < T_p$. Thus, when a layer of the ground material becomes frozen the total water content ζ in it stays constant until the moment when the layer becomes thawed again. Note that for frozen soil layers the matric potential can be arbitrarily defined, since it does not enter into calculations, and the water flux boundary condition is imposed at the bottom of the thawed region.

In many practical applications, heat conduction is the dominant mode of energy transfer in a ground material. Within certain assumptions (Andersland and Anderson, 1978) the soil temperature $T, [^\circ C]$ can be simulated by a 1-D heat equation with phase change (Carslaw, 1974):

$$C\frac{\partial}{\partial t}T(x,t) + L\zeta\frac{\partial}{\partial t}\theta(T,x) = \frac{\partial}{\partial x}\lambda\frac{\partial}{\partial x}T(x,t), \quad x \in [x_s, x_b], \quad t \in [0,\tau]. \tag{14}$$

The quantities C=$C(T,x)$ $[Jm^{-3}K^{-1}]$ and λ=$\lambda(T,x)$ $[Wm^{-1}K^{-1}]$ represents the volumetric heat capacity and thermal conductivity of soil, respectively; L $[Jm^{-3}]$ is the volumetric latent heat of fusion of water, ζ is the volumetric water content, and θ is the unfrozen liquid pore water fraction. The volumetric water content ζ=$\eta\psi$, where η is the

soil porosity and $\psi \in [0,1]$ is the fraction of voids filled with water. The latter can be obtain by solving the Richard's equation (see equation 13 in subsection).

The heat equation is supplemented by initial temperature distribution $T(x_s,0)$=$T_0(x)$, and boundary conditions at the snow/ground surface x_s and at the depth x_b. Here, $T_0(x)$ is the temperature at $x \in [x_s, x_b]$ at time t=0; T_{air} is observed air temperatures at the ground/snow surface, respectively. We use the Dirichlet boundary conditions at the snow surface, i.e. $T(x_s,t)$=$T_{air}(t)$, and a heat flux boundary condition at the bottom of the soil column $\lambda \nabla T(l,t)$=$\mathcal{G}$, where $\mathcal{G}$ is the geothermal heat flux. In the model, we assume that the lower boundary x_b is located at 60.0 meters that is adequate to simulate the temperature dynamics on the decadal scale (Alexeev et al., 2007).

The model uses parametrizations of thermal properties proposed by (DeVries, 1963; Sass et al., 1971), with modifications for the thermal conductivity λ_m as well as the heat capacity C_m for the mineral soil by

$$\lambda_m = \lambda_s^{1-\eta} \left[\lambda_a^{1-\psi} \lambda_w^{\psi}\right]^{\eta}, \quad \lambda_w = \lambda_l^{\theta} \lambda_i^{1-\theta},$$

and

$$C_m = (1-\eta)C_s + \eta\left[(1-\psi)C_a + \psi C_w\right], \quad C_w = \theta C_l + (1-\theta)C_i,$$

where C_k and λ_k, $k \in \{a, w, i, s\}$ are the volumetric heat capacities and the thermal conductivities of the k^{th} component, respectively. Subscripts 's', 'a', 'w', 'l', and 'i' stand for the mineral skeleton, air, water, liquid water and ice, respectively.

Recall that the value of $\theta \in [0,1]$ stands for the unfrozen liquid pore water fraction. There are many approximations to θ in the fully saturated soil (ψ=1). The most common approximations are associated with power or exponential functions. Based on our positive experience, we parameterize θ by a power function $\theta(T)$=$a|T|^{-b}; a, b$>0 for T<T_*<0°C. The constant T_* is called the freezing point depression. On other hand, in thawed soils (T>T_*), all pore water is liquid and θ=1. We thus hypothesize that

$$\theta = \begin{cases} 1, & T \geq T_* \\ |T_*|^b |T|^{-b}, & T < T_* \end{cases}, \tag{15}$$

is valid both for the saturated and partially saturated soils. Small values of b describe the liquid water content in fine-grained soils, whereas large values of b are related to coarse-grained materials in which almost all water freezes at the temperature T_*.

For the sake of computational efficiency, the soil column is discretized $[0, x_b]$ into 22 layers, and the snow pack $[x_s, 0]$ into up to five layers. The number of the snow layers depends on the value of x_s. Following Lawrence and Slater (2008), soil thermal and hydraulic properties (e.g. λ, and C) for the i-th layer are a weighted combination of organic and mineral soil properties $\mathcal{P}_i = (1-f_i)\mathcal{P}_m + f_i \mathcal{P}_o$, where f_i is the fraction of organic material in the i-th soil layer, $\mathcal{P}_m$ is the value for mineral soil, $\mathcal{P}_o$ is the value for organic soil, and $\mathcal{P}_i$ is the weighted average quantity.

The Global Soil Data Task (GSDT, 2000) data set contains soil-carbon density (C, kg m^{-3}) across the depth interval of 0–1 m. To obtain C across the pan-Arctic basin we averaged the five arc-second GSDT data for each EASE-Grid cell. We applied the soil profile for polar and boreal soils from Zinke et al. (1986) to obtain carbon storage over the top 11 model soil layers (1.4 m depth). Soil carbon or organic fraction for each layer was then determined as

$$f_{sc,i} = \rho_{sc,i} / \rho_{sc,max} \tag{16}$$

where $f_{sc,i}$ is the carbon fraction of each layer i, $\rho_{sc,i}$ is the soil carbon density and $\rho_{sc,max}$ is the maximum possible value (peat density of 130 kg m^3, Forouki (1981)). Soil properties for each layer are specified as a weighted combination of organic and mineral soil properties

$$\mathcal{P} = (1 - f)\mathcal{P}_m + f\mathcal{P}_o \tag{17}$$

where f is the fraction of organic material in the soil layer, $\mathcal{P}_m$ is the value for mineral soil, $\mathcal{P}_o$ is the value for organic soil, and $\mathcal{P}$ is the weighted average quantity. Thermal and hydrologic parameters as a function of soil class are listed in Table 1.

2.3. **Soil Water and Runoff.** The temperature of a soil model layer affects the amount of soil water (θ) which changes phase (melt or freeze) each day of the simulation. Infiltration into the first soil layer occurs when there is water in the surface pool θ_0, or when there is residual of water at the surface

$$q_{in} = q_{liq} - q_{over} - q_{evap} \tag{18}$$

where θ_0 is water in the surface pool (mm), or precipitation plus any snowmelt water (mm day^{-1}), q_{over} is overland runoff, and q_{evap} is evaporation from the surface pool. The surface pool thus loses water via overland runoff and evaporation. Adjustable rate parameters influence q_{over}. Evaporation from the surface pool occurs at the PET rate (B_t). q_{over} is estimated as

$$q_{over} = q_{liq} \cdot k_{over} \tag{19}$$

where k_{over} (dimensionless) is an adjustable rate coefficient (Table 2). The maximum infiltration rate ($q_{in,max}$, mm day^{-1}) is defined by

$$q_{in,max} = q_0 \cdot (1 - \theta_{liq}/\theta_{max}) \tag{20}$$

where q_0 is the maximum rate when no liquid water is present, θ_{liq} is the liquid water content (mm), and θ_{max} is soil layer capacity (mm). Water flow between soil layers is governed by Darcy's law

$$q = -k\frac{\partial \psi_h}{\partial z} \tag{21}$$

where k is the hydraulic conductivity (mm s^{-1}), ψ_h is the hydraulic potential (mm), and z is depth. The scheme for soil water movement is solved numerically through a modified version of the Richard's equation (Zeng and Decker, 2009)

$$\frac{\partial \theta}{\partial t} = \frac{\partial}{\partial z}\left[k\left(\frac{\partial(\psi - \psi_E)}{\partial z}\right)\right] - Q \tag{22}$$

at time t, where Q is a soil moisture sink term representing ET flux loss (mm of water mm^{-1} of soil s^{-1}).

Total daily runoff is the sum of surface runoff from the surface water pool, precipitation or snowmelt greater than infiltration capacity, and excess water in one or more soil layers (baseflow or 'subsurface' runoff). Baseflow is a proportion of the excess water in a soil layer i

$$q_{base,i} = (q_i - FC_i) \cdot k_{base} \tag{23}$$

2.4. **Evapotranspiration.** Daily simulated ET (mm day^{-1}) for each grid cell in the model domain depends on atmospheric demand, and surface and soil conditions

$$\hat{ET} = PET\, F_{roots}\, F_{water} \tag{24}$$

where $\hat{ET}$ is unadjusted ET (mm day^{-1}), PET is potential evapotranspiration (mm day^{-1}), F_{roots} is the proportion of roots in the soil layer, and F_{water} is the proportion of water above field capacity relative to the available storage in the soil layer. PET can be estimated using the Hamon function (equation 1) or the Penman-Monteith method (Monteith, 1965). Simulations with the Hamon function require fewer daily time series forcing data, and less compuational expense, compared to the Penmen-Monteith method. When using the Hamon function, a calibration coefficient (k_{ET}) is applied to account for spatial variations in canopy conductance and to scale the daily grid ET, with the assumption that canopy conductance is equal to surface conductance:

$$ET = \hat{ET}\, k_{ET} \tag{25}$$

Soil layers within the depth of ground deemed the rooting zone are subject to vertical water losses to the atmosphere via evapotranspiration (ET). The fraction of roots in these soil layers are estimated obtained using the function of Jackson et al. (1996)

$$Y = 1 - \beta^d \tag{26}$$

where Y is the cumulative root fraction with depth (a proportion between 0 and 1), d is soil depth (in cm), and β is the fitted parameter, with larger values implying a deeper rooting profile. For general applications across the pan-Arctic where relatively shallower rooting depths the value of $\beta = 0.943$ is used (Jackson et al., 1996).

2.5. **Numerical implementation for soil moisture calculations.** The numerical implementation for water movement across soil layers involves a series of equations that are solved as a tridiagonal set (REF Press). The boundary condition for the first soil layer ($i = 1$) is the infiltration rate ($q_{i-1}^{n+1} = -q_{in}^{n+1}$), where n is the time increment. This establishes a water balance of

$$\frac{\Delta z_i \Delta \theta_{liq,i}}{\Delta t} = q_{in}^{n+1} + q_i^{n+1} - e_i \tag{27}$$

Coefficients for the tridiagonal set for $i = 1$ are

$$a_i = 0 \tag{28}$$

$$b_i = \frac{\partial q_i}{\partial \theta_{liq,i}} - \frac{\Delta z_i}{\Delta t} \tag{29}$$

$$c_i = \frac{\partial q_i}{\partial \theta_{liq,i}} \tag{30}$$

$$r_i = q_{in}^{n+1} - q_i^n + e_i \tag{31}$$

The coefficients of the set for soil layers $i = 2, ..., N-1$ are

$$a_i = \frac{\partial q_{i-1}}{\partial \theta_{liq,i-1}} \tag{32}$$

$$b_i = \frac{\partial q_i}{\partial \theta_{liq,i}} - \frac{\partial q_{i-1}}{\partial \theta_{liq,i}} - \frac{\Delta z_i}{\Delta t} \tag{33}$$

$$c_i = \frac{\partial q_i}{\partial \theta_{liq,i+1}} \tag{34}$$

$$r_i = q_{i-1}^n - q_i^n + e_i \tag{35}$$

A zero-flux bottom boundary condition (q_i^n) is imposed for the lowest soil layer, which gives a tridiagonal set of

$$a_i = -\frac{\partial q_{i-1}}{\partial \theta_{liq,i-1}} \tag{36}$$

$$b_i = \frac{\partial q_{i-1}}{\partial \theta_{liq,i}} - \frac{\Delta z_i}{\Delta t} \tag{37}$$

$$c_i = 0 \tag{38}$$

$$r_i = q_{i-1}^n + e_i \tag{39}$$

Liquid water contents for each layer $i = 1, ...N$ are subsequently updated

$$w_{liq,i}^{n+1} = w_{liq,i}^n + \Delta\theta_{liq,i}\Delta z_i \tag{40}$$

2.6. **Numerical discretization for soil temperature calculations.** Following finite element framework (Zienkiewicz and Taylor, 1991), we approximate $T(x,\tau) \approx \sum_{i=1}^n \phi_i(x)\mathbf{t}_i(\tau)$, where $\mathbf{t}_i(\tau)$ is a "value" of temperature at the i-th finite element grid, and ϕ_i is the so-called basis function. After some standard manipulations, we derive a system of differential equations

$$\mathbf{M}(\mathbf{t})\frac{d}{d\tau}\mathbf{t}(\tau) = -\mathbf{K}(\mathbf{t})\mathbf{t}(\tau), \qquad \mathbf{t} = \mathbf{t}(\tau), \tag{41}$$

where $\mathbf{t}(\tau) = \{\mathbf{t}_i(\tau)\}_{i=1}^n$ is the vector consisting of temperature values, $\mathbf{M}(\mathbf{t}) = \{m_{ij}(\mathbf{t})\}_{ij=1}^n$ and $\mathbf{K}(\mathbf{t}) = \{k_{ij}(\mathbf{t})\}_{ij=1}^n$ are the $n \times n$ capacitance and stiffness matrices, respectively. A further refinement, which is often used in finite element modeling of phase change problems, is to exploit a so-called "lumped" formulation, i.e. the capacitance matrix $\mathbf{M}$ is diagonal:

$$m_{ij}(\mathbf{t}) = \delta_{ij}c_i(\mathbf{t})\int_0^l \psi_i dx, \qquad c_i(\mathbf{t}) \approx C(\mathbf{t}_i, x_i) + L\zeta_i\frac{d\theta}{dT}(\mathbf{t}_i), \tag{42}$$

where δ_{ij} is one if $i = j$, or zero otherwise. Dalhuijsen and Segal (1986) provides justification for the lumped formulation on noting that it is computationally advantageous and avoids oscillations in numerical solutions when used in conjunction with the backward Euler scheme:

$$\begin{aligned} \left[\mathbf{M}^{(k)} + d\tau_k\mathbf{K}^{(k)}\right]\mathbf{t}^{(k)} &= \mathbf{M}^{(k)}\mathbf{t}^{(k-1)}, & k > 1 \\ \mathbf{t}^{(k)} &= \mathbf{t}_0, & k = 0. \end{aligned} \tag{43}$$

TABLE 2. Adjustable parameters for snow and soil processes. Quantities marked with a - are dimensionless.

Rain/Snow threshold	t_{thresh}	°C
Snow sublimation	G_t	-
Snowpack ripening	$k_{swehold}$	%
Snowpack release	k_{sweout}	%
Infiltration maximum	q_0	%
Baseflow	k_{base}	%

The main difficulty in numerical modeling of soil freezing/thawing is in consistent calculation of the derivative $d\theta/dT$ in (42), where $\theta(T)$ is not a continuously differentiable function defined by (15). In many reviews, it is proposed to employ the *enthalpy temporal averaging* to calculate $c_i(\mathbf{t})$. We suggest an approach that incorporates ideas of temporal averaging just to evaluate the rapidly changing $\theta(T)$ by defining c_i as

$$c_i(\mathbf{t}^{(k)}) = C(\mathbf{t}_i^{(k)}, x_i) + L\frac{\theta_r(\mathbf{t}_i^{(k)}) - \theta_r(\mathbf{t}_i^{(k-1)})}{\mathbf{t}_i^{(k)} - \mathbf{t}_i^{(k-1)}}. \tag{44}$$

We note that an advantage of this definition is that it does not compute temporal averaging of the heat capacity, and hence reduces numerical computations, and at the same time preserves numerical accuracy of the original idea. Studies described in Nicolsky et al. (2007, 2009) provide further details about the phase change computations.

3. Algorithms for Processes Involving Dissolved Organic Carbon

The model was recently extended to simulate the production, decomposition, and leaching of dissolved organic carbon (DOC). Production of DOC is assumed to occur through incomplete decomposition of soil organic matter (SOM), with the rate of decomposition, and thus DOC production, influenced by soil temperature, soil moisture, and the amount of soil organic matter (SOM) (McGuire et al., 2010; Kicklighter et al., 2013). DOC production occurs as follows:

$$r_p(t) = k_{prod}\, SOM\, f(T)\, f(S_w) \tag{45}$$

where r_p(t) is the rate of DOC production (g C m^2 day^{-1}) on day t, k_{prod} represents the production rate coefficient (day^{-1}), SOM is the density of soil organic matter (g C m^{-2}, and $f(T)$ and $f(S_w)$ are the rate dependence on soil temperature (T) and moisture (S_W), respectively. Table 3 lists the adjustable parameters for DOC production and decomposition. The influence of soil temperature on DOC production in each soil layer is modeled through the commonly used Q_{10} relationship: $f(T) = Q_{10}^{|T-10|/10}$, where Q_{10} estimates the rate increases with soil temperature. The influence of soil moisture is modeled with $f(S_w) = (S_w)^n$, where n takes the value of 1.0, which is within the typical range of 0.75–3.0 for most soils (Yan et al., 2018). For each model soil layer, SOM densities are drawn from the 0–100, 100–200, or 200–300 cm layer value in the Northern Circumpolar Soil Carbon Database (NCSCD v2.2) (Hugelius et al., 2013).

Decomposition of DOC is assumed to be lost to carbon dioxide and/or sorbed to the mineral soil as expressed by

$$BIO(t) = k_{decomp}\, S_{DOC}(t) \tag{46}$$

where k_{decomp} decomposition rate coefficient (day^{-1}). Estimates of daily DOC production (equation 45) and loss to decomposition (equation 46) are used to update the soil DOC pool

$$S_{DOC}(t) = S_{DOC}(t-1) + r_p - BIO(t) \tag{47}$$

where $S_{DOC}(t)$ is soil DOC storage (g C m^2).

Melt water accumulating at the base of warming snowpacks in late spring (late-April to early-May) interacts with soil organic carbon in decaying vegetation and shallow organic-rich soil layers, including biomass produced during the prior growing season (Spencer et al., 2008; Guo and Macdonald, 2006; Neff et al., 2006). To account for the high DOC concentration during peak flows, the SOM values for surface leaching are scaled from the NCSCD 0–100 cm data value when there is water in the snowpack or meltwater at the surface. The k_{prod} is also modified during these snowwater and meltwater events. The scaling factor ($\mathcal{L}$) is set under the following conditions when snowpack liquid water is present, and for the N meltwater events:

$$\mathcal{L} = \begin{cases} \mathcal{L}_1 & \text{if } N = 1 \text{ to } 3 \text{ or snowpack water present} \\ \mathcal{L}_2 & \text{if } N = 4 \text{ to } 6 \\ \mathcal{L}_3 & \text{if } N = 7 \text{ to } 10 \end{cases} \tag{48}$$

In Rawlins et al. (2021), $\mathcal{L}_1$, $\mathcal{L}_2$, and $\mathcal{L}_3$ were assigned values of 6.0×10^2, 5.0×10^2, and 4.0×10^2, respectively. The modifications to surface SOM and production reflect the relatively high DOC yield that occurs during the spring freshet. Transfer of DOC from soils to stream and river networks takes place whenever surface or subsurface runoff occurs

$$DOC(t) = S_{DOC}(t)\, Q \tag{49}$$

where DOC(t) is mass load (g C m^2 day^{-1}) and Q is runoff (m day^{-1}).

TABLE 3. Adjustable parameters for DOC production and loading from surface and within soils. Surface k_{prod} are scaled to account for enhanced production and leaching during and after snowmelt as described by equation 48. In Rawlins et al. (2021) the parameters were set separately for the Mackenzie, Yukon, and for the remainder of river basins in the western Arctic study domain.

DOC parameters	
Parameter	**Description**
$k_{prod,sub}$	DOC production rate coefficient, subsurface
$k_{prod,surf}$	DOC production rate coefficient, surface
$k_{decomp,sub}$	DOC decomposition rate coefficient, subsurface
$k_{decomp,surf}$	DOC decomposition rate coefficient, surface

References

Alexeev, V., Nicolsky, D., Romanovsky, V., and Lawrence, D. (2007). An evaluation of deep soil configurations in the clm3 for improved representation of permafrost. *Geophys. Res. Lett.*, 34(9).

Andersland, O. and Anderson, D. (1978). *Geotechnical engineering for cold regions*. McGraw-Hill.

Carslaw, H. (1974). S and Jaeger J C 1959 Conduction of Heat in Solids. *Oxford University Press, New York*, 302:340–341.

Dalhuijsen, A. and Segal, A. (1986). Comparison of finite element techniques for solidification problems. *International journal for numerical methods in engineering*, 23(10):1807–1829.

DeVries, D. (1963). Thermal properties of soils, Physics of Plant Environment WR Van Wijk.

Federer, C. A. and Lash, D. (1978). Brook: A hydrologic simulation model for eastern forests. Technical report, University of New Hampshire Water Resources Research Center *Research Report* No. 19.

Forouki, O. T. (1981). Thermal properties of soils. Technical report, CRREL. Report No. Vol. 81, No. 1, CRREL Monograph.

Global Soil Data Task (2000). Global gridded surfaces of selected soil characteristics (IGBPDIS). Available online [http://www.daac.ornl.gov/] from the ORNL.

Guo, L. and Macdonald, R. W. (2006). Source and transport of terrigenous organic matter in the upper yukon river: Evidence from isotope (δ13c, δ14c, and δ15n) composition of dissolved, colloidal, and particulate phases. *Global Biogeochemical Cycles*, 20(2).

Hamon, W. R. (1963). Computation of Direct Runoff Amounts from Storm Rainfall. *Int. Assoc. Sci. Hydrol. Publ.*, 63:52–62.

Hinzman, L. D. and Kane, D. L. (1991). Snow Hydrology of a Headwater Arctic Basin 2. Conceptual analysis and Computer modeling. *Water Resour. Res.*, 27(6):1111–1121.

Hugelius, G., Tarnocai, C., Broll, G., Canadell, J., Kuhry, P., and Swanson, D. (2013). The Northern Circumpolar Soil Carbon Database: spatially distributed datasets of soil coverage and soil carbon storage in the northern permafrost regions. *Earth System Science Data*, 5(1):3–13.

Jackson, R., Canadell, J., Ehleringer, J. R., Mooney, H., Sala, O., and Schulze, E. D. (1996). A global analysis of root distributions for terrestrial biomes. *Oecologia*, 108(3):389–411.

Kicklighter, D. W., Hayes, D. J., McClelland, J., Peterson, B. J., McGuire, A. D., and Melillo, J. M. (2013). Insights and issues with simulating terrestrial DOC loading of arctic river networks. *Ecological Applications*. in press.

Lawrence, D. M. and Slater, A. G. (2008). Incorporating organic soil into a global climate model. *Clim. Dynam.*, 30. DOI 10.1007/s00382-007-0278-1.

Liston, G. E., Haehnel, R. B., Sturm, M., Hiemstra, C. A., Berezovskaya, S., and Tabler, R. D. (2007). Simulating complex snow distributions in windy environments using SnowTran-3D. *Journal of Glaciology*, 53(181):241–256.

Lunardini, V. J. (1978). Theory of N-factor and correlation of data. In *Proceedings of the Third International Conference on Permafrost*, volume 1, pages 40–46. National Council of Canada, Ottawa.

Lunardini, V. J. (1981). *Heat Transfer in Cold Climates*. Van Nostrand Reinhold, New York. 731 pp.

Mao, J. and Yan, B. (2019). Global monthly mean leaf area index climatology, 1981-2015. Technical report, ORNL DAAC, Oak Ridge, Tennessee, USA.

McGuire, A. D., Hayes, D. J., Kicklighter, D. W., Manizza, M., Zhuang, Q., Chen, M., Follows, M. J., Gurney, K. R., McClelland, J. W., Melillo, J. M., et al. (2010). An analysis of the carbon balance of the Arctic Basin from 1997 to 2006. *Tellus B*, 62(5):455–474.

Monteith, J. L. (1965). Evaporation and Environment. In *The State and Movement of Water in Living Organisms*, pages 205–233. Cambridge University Press, Cambridge UK. G. E. Fogg, Ed.

Neff, J., Finlay, J., Zimov, S., Davydov, S., Carrasco, J., Schuur, E., and Davydova, A. (2006). Seasonal changes in the age and structure of dissolved organic carbon in siberian rivers and streams. *Geophysical Research Letters*, 33(23).

Nicolsky, D., Romanovsky, V., Alexeev, V., and Lawrence, D. (2007). Improved modeling of permafrost dynamics in a GCM land-surface scheme. *Geophys. Res. Lett*, 34:L08501.

Nicolsky, D., Romanovsky, V., and Panteleev, G. (2009). Estimation of soil thermal properties using in-situ temperature measurements in the active layer and permafrost. *Cold Regions Science and Technology*, 55(1):120–129.

Rawlins, M., Nicolsky, D., McDonald, K., and Romanovsky, V. (2013). Simulating soil freeze/thaw dynamics with an improved pan-arctic water balance model. *JAMES*, 5(4):659–675.

Rawlins, M. A., Connolly, C. T., and McClelland, J. W. (2021). Modeling terrestrial dissolved organic carbon loading to western Arctic rivers. *J. Geophys. Res.-Biogeo.* in review.

Rawlins, M. A., Lammers, R. B., Frolking, S., Fekete, B. M., and Vörösmarty, C. J. (2003). Simulating Pan-Arctic Runoff with a Macro-Scale Terrestrial Water Balance Model. *Hydrol. Process.*, 17:2521–2539.

Sass, J., Lachenbruch, A. H., and Munroe, R. J. (1971). Thermal conductivity of rocks from measurements on fragments and its application to heat-flow, determinations. *Journal of Geophysical Research*, 76(14):3391–3401.

Schaefer, K., Zhang, T., Slater, A. G., Lu, L., Etringer, A., and Baker, I. (2009). Improving simulated soil temperatures and soil freeze/thaw at high-latitude regions in the Simple Biosphere/Carnegie-Ames-Stanford Approach model. *J. Geophys. Res.*, 114(F02021).

Spencer, R. G., Aiken, G. R., Wickland, K. P., Striegl, R. G., and Hernes, P. J. (2008). Seasonal and spatial variability in dissolved organic matter quantity and composition from the Yukon River basin, Alaska. *Global Biogeochemical Cycles*, 22(4).

Sturm, M., Holmgren, J., König, M., and Morris, K. (1997). The thermal conductivity of seasonal snow. *Journal of Glaciology*, 43(143):26–41.

Sturm, M. J., Holmgren, J., and Liston, G. E. (1995). A seasonal snow cover classification system for local to global applications. *J. Climate*, 8(5):1261–1283.

Vörösmarty, C. J., Federer, C. A., and Schloss, A. L. (1998). Potential Evapotranspiration Functions Compared on US Watersheds: Possible Implications for Global-Scale Water Balance and Terrestrial Ecosystem Modeling. *J. Hydrol.*, 207:147–169.

Willmott, C. J., Rowe, C. J., and Mintz, Y. (1985). Climatology of the Terrestrial Seasonal Water Cycle. *J. Climate*, 5:589–606.

Yan, Z., Bond-Lamberty, B., Todd-Brown, K. E., Bailey, V. L., Li, S., Liu, C., and Liu, C. (2018). A moisture function of soil heterotrophic respiration that incorporates microscale processes. *Nature communications*, 9(1):1–10.

Zeng, X. and Decker, M. (2009). Improving the numerical solution of soil moisture–based richards equation for land models with a deep or shallow water table. *Journal of Hydrometeorology*, 10(1):308–319.

Zienkiewicz, O. and Taylor, R. (1991). The Finite Element Method, Vol. 2 (Solid and Fluid Mechanics, Dynamics and Nonlinearity). *McGraw-Hill*, 620:227–229.

Zinke, P. J., Stangenberger, A. G., Post, W. M., Emanuel, W. R., and Olson, J. S. (1986). Worldwide organic carbon and nitrogen data. Technical report, Carbon Dioxide Information Center, Oak Ridge, Tennessee. ORNL/ CDIC-18.